Experimental and Theoretical Analysis of CO2 Absorption in Polyolester Oil Using the PC−SAFT Equation of State to Account for Nonideal Effects

ARTICLE *in* INDUSTRIAL & ENGINEERING CHEMISTRY RESEARCH · JANUARY 2012

Impact Factor: 2.59 · DOI: 10.1021/ie2011752

2 AUTHORS:

Moises A. Marcelino Neto
Federal University of Santa Catarina
27 PUBLICATIONS **100** CITATIONS
SEE PROFILE

Jader R Barbosa Jr.
Federal University of Santa Catarina
204 PUBLICATIONS **725** CITATIONS
SEE PROFILE

I&EC research
Industrial & Engineering Chemistry Research

ARTICLE

pubs.acs.org/IECR

Experimental and Theoretical Analysis of CO_2 Absorption in Polyolester Oil Using the PC-SAFT Equation of State to Account for Nonideal Effects

Moisés A. Marcelino Neto and Jader R. Barbosa, Jr.*

Polo—Research Laboratories for Emerging Technologies in Cooling and Thermophysics Department of Mechanical Engineering, Federal University of Santa Catarina, Florianópolis, Santa Catarina 88040900, Brazil

ABSTRACT: The purpose of this work is to study the absorption of carbon dioxide (CO_2) through the free surface of a stagnant layer of polyolester oil in a closed cell via the pressure decay method. The system pressure and local temperatures in the vapor and liquid phases were recorded as a function of time for system temperatures of 25, 40, 55, and 70 °C. The tests were carried out for two initial heights of the liquid layer of 37 and 74 mm, respectively. The mass of CO_2 that entered the cell was measured for each test. The data were used to validate a transient mass diffusion model that accounts for the departure from the ideal behavior. The model uses the PC-SAFT equation of state and incorporates the following nonideal effects: (i) gas compressibility in the vapor, (ii) liquid phase swelling, (iii) concentration-dependent nonideal density behavior, (iv) nonideal phase equilibrium at the vapor−liquid interface, and (v) concentration-dependent mass diffusivity. Absorption rates were found to be strongly dependent on, and inversely proportional to, the system temperature. The absolute average errors of the absolute pressure prediction were lower than 4%. When the nonideal effects are ignored, the absolute average errors can be as large as 30%.

INTRODUCTION

Because of their environmentally friendly characteristics, the past two decades have seen renewed interest in natural refrigerants, such as water, carbon dioxide, ammonia, and hydrocarbons. Despite the high pressures found in its applications as a primary refrigerant, carbon dioxide (CO_2) may still be a promising alternative for automotive air conditioning, heat pumps and light commercial mechanical vapor compression refrigeration applications.

Equilibrium thermodynamics of mixtures of CO_2 and several types of lubricants used in refrigeration compressors has been the subject of experimental and modeling studies.[1−7] However, very little information is available regarding the transient mass transfer processes that take place during absorption of CO_2 in lubricant oil. In general, detailed knowledge of absorption of gaseous refrigerant in lubricant oil is important for determining the refrigeration system equalizing pressure (i.e., the system pressure before the compressor start-up) and the compressor performance during cyclic operation.

Liquid CO_2 is lighter than ester-based lubricants. Thus, the process of CO_2 absorption in the compressor oil sump is governed by molecular diffusion. In refrigeration applications, several papers describe the mechanisms of absorption of hydrocarbons and hydrofluorocarbons in oil.[8−14] Fukuta et al.[15] discussed the transient mixing of a mixture of isobutane and mineral oil at constant pressure. In their one-dimensional diffusion model, the mass diffusivity was assumed independent of concentration and the solution density was assumed constant. Barbosa and Ortolan[16] evaluated experimentally the absorption of R-134a and isobutane in oil layers of different thicknesses. Three polyolester (POE) oils of different viscosity grades were used. For the R-134a-POE systems, a macroscopic control volume model based on the solution of mass balance equations for the vapor and liquid phases was proposed. For the isobutane-oil mixtures, the data were correlated with an empirical expression based on the Buckingham-Pi theorem. More recently, Marcelino Neto and Barbosa[14] studied the absorption of isobutane through the free surface of a stagnant layer of alkylbenzene (AB) oil in a transparent PVT cell. The tests were conducted at 25, 40, 55, and 70 °C. The experimental data were used to validate a transient mass diffusion model that took into account the departure from ideal solution behavior via the Peng and Robinson[17] equation of state (EoS).

In the particular case of CO_2, several works were carried out to investigate its absorption in nonvolatile liquids for petroleum engineering applications.[18−20] Most of these studies consisted of transient one-dimensional models that consider constant temperature, negligible convection effects, constant mass diffusivity, ideal gas, and negligible liquid swelling. A detailed review of such studies was made available in a recent paper.[14] Okhotsimskii and Hozawa[21] carried out a visualization study (via the Schlieren technique) of CO_2 absorption and desorption in sixteen organic systems. The systems were classified according to their stability with respect to density and surface tension effects (Rayleigh and Marangoni numbers) that, in turn, dictate the occurrence of interfacial turbulence and cellular flow. CO_2 absorption in ionic liquids has also been researched with the purpose of finding effective solvents for carbon sequestration.[22−24]

In this paper, absorption of CO_2 through the free surface of a stagnant layer of POE ISO 68 lubricant oil in a closed system is investigated experimentally for two heights of the oil

Received: June 2, 2011
Accepted: December 5, 2011
Revised: November 18, 2011
Published: December 05, 2011

dx.doi.org/10.1021/ie2011752 | *Ind. Eng. Chem. Res.* 2012, 51, 1027–1035

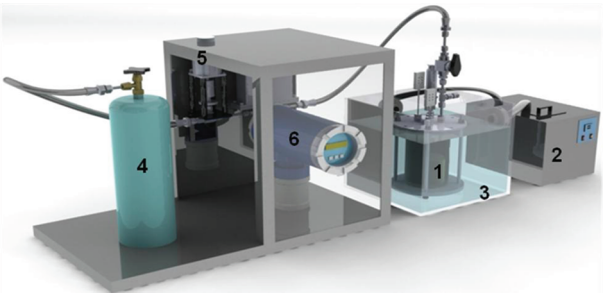

Figure 1. Experimental apparatus: (1) test cell, (2) thermostatic bath, (3) water tank, (4) CO_2 reservoir, (5) automatic needle valve, and (6) Coriolis mass flow meter.

layer (37 and 74 mm). The test section was specially constructed to enable measurement of the instantaneous pressure, liquid and vapor temperatures and the mass of CO_2 that enters the cell (initially held in vacuum). In the mathematical model proposed for calculating the pressure decay, the departure from the ideal solution behavior is dealt with via the PC-SAFT EoS.[25] The model takes into account the gas compressibility, liquid phase swelling, nonideal concentration-dependent density behavior, nonideal phase equilibrium behavior at the interface, and concentration-dependent mass diffusivity by means of thermodynamic models for the CO_2−POE ISO 68 mixture.[7] CO_2 absorption rates were found to be strongly dependent on, and inversely proportional to, the system temperature. As will be seen, a comparison of the instantaneous pressure calculated with the proposed model with experimental data is presented, and absolute average errors smaller than 4% are observed. Much larger absolute average errors (of the order of 20% in most cases, but as large as 30% in the worst case) are obtained when the nonideal effects are ignored. Liquid swelling was found to be more significant for the 37 mm case.

EXPERIMENTAL WORK

The experimental facility shown in Figure 1 consists of a 190-mm high, 120-mm ID stainless steel cylindrical tank equipped for absolute pressure and temperature measurements. Temperatures are recorded by three Pt-100 resistance temperature detectors (RTDs) located at three different heights in the cylinder. The sensors nearest to the top and to the bottom of the cylinder measure the temperatures of the gas (T_G) and of the liquid (T_L), respectively. The tip of the intermediate sensor is located at the position occupied by the gas−liquid interface at the beginning of the experiment. Therefore, it is expected that it will record, at least during the early stages of absorption (when the temperature variation is more pronounced and when liquid swelling has not altered the liquid volume substantially), the interface temperature (T_I). The measurement uncertainties of pressure and temperature are ±15 kPa and ±0.15 °C, respectively.

Initially, a specified amount of oil is placed in the cell (1) and vacuum is produced in the apparatus to take out moisture and dissolved gases. The vacuum generated in the experimental apparatus was such that the absolute pressure prior to an experimental test is of the order of 4 Pa. The system temperature is set by a thermostatic bath (2) that circulates service water through a tank (3) in which the test cell is immersed. CO_2 vapor is kept at thermodynamic equilibrium with its liquid at room temperature

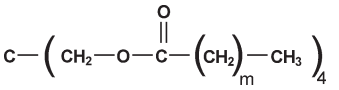

Figure 2. Molecular structure of the polyol ester lubricant oil (m = 8).

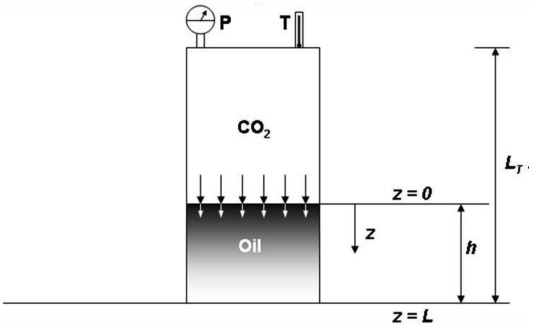

Figure 3. Mathematical model geometry.

(24 °C, approximately) inside a 2 L reservoir (4). An automatic needle valve (5) that connects the reservoir to the test cell is opened slowly for a specified amount of time (typically 8 s). This time allows equalization of pressures between the reservoir and the test cell. The mass of vapor that enters the test cell is measured by a Coriolis mass flow meter (6) with an error of ±0.15% of the absolute reading. The valve is closed automatically and the pressure in the cell decreases with time as result of CO_2 absorption in the lubricant oil layer.

The absorption experiments were performed at 25, 40, 55, and 70 °C (nominal) for initial heights of the oil layer of 37 and 74 mm. CO_2 was supplied by AGA with 99.99% purity. The molecular structure of the POE is shown in Figure 2. The number of molecular groups, m, was determined to be equal to 8 so as to satisfy the value of the approximate molecular weight supplied by the manufacturer (760 g mol^{-1}). The lubricant mass density at 20 °C and its kinematic viscosity at 40 °C are 972.6 kg m^{-3} and 68.5 mm^2 s^{-1}, respectively.[7] The purity of the lubricant was not available in the manufacturer data sheet, which informed the total acid number (0.02 mg KOH/g) and the water content (25 ppm) of a typical sample. The oil was used as delivered and there were no additives in the sample.

MODELING

Mass Diffusion in the Liquid Phase. A general approach for solving the mass diffusion problem was formulated based on the species conservation equation. A schematic illustration of the CO_2−POE system is shown in Figure 3, where the vapor−liquid interface is located at $z = 0$, and the bottom of the cell is at $z = L$.

The mass diffusion process is considered isothermal. Density-induced (Rayleigh) convection is assumed nonexistent due to the fact that the lubricant is heavier than liquid CO_2. Surface tension-induced (Marangoni) convection effects are ignored. Thus, based on Fick's Law, CO_2 diffusion in the liquid layer can be calculated via the following equation,

$$\frac{\partial w_1}{\partial t} + \frac{1}{L}\frac{dL}{dt}\frac{\partial w_1}{\partial \alpha} = \frac{1}{\rho_L L^2}\frac{\partial}{\partial \alpha}\left(\rho_L D_{12}\frac{\partial w_1}{\partial \alpha}\right) \quad (1)$$

where w_1 is the mass fraction of CO_2 in the liquid, t is time, z is the distance from the interface and α is the normalized distance

dx.doi.org/10.1021/ie2011752 |Ind. Eng. Chem. Res. 2012, 51, 1027–1035

Table 1. PC-SAFT Parameters for Pure Components

component	T range (K)	m_i	σ_i (Á)	ε_i/κ
CO_2	216−304	2.0729	2.7852	169.21
POE ISO 68	293−403	11.1356	4.7572	301.87

from the free interface given by

$$\alpha = \frac{z}{L} \tag{2}$$

where L is the instantaneous height of the liquid layer, whose increase due to liquid swelling is accounted for via the second term on the left-hand side of eq 1. ρ_L is the solution mass density and D_{12} is the liquid mass diffusivity. As the oil is initially under vacuum, the initial condition is given by

$$w_1(\alpha, t)|_{t=0} = 0 \tag{3}$$

At the bottom of the test cell, the mass flux at any time is equal to zero. Thus

$$\left.\frac{\partial w_1(\alpha, t)}{\partial \alpha}\right|_{\alpha=1} = 0 \tag{4}$$

Thermodynamic equilibrium was assumed at the vapor−liquid interface. Therefore

$$w_1(\alpha, t)|_{\alpha=0} = w_1^{\text{sat}}[p(t)] \tag{5}$$

where p is the instantaneous pressure. The initial height of the liquid layer, L_0, is equal to 37 or 74 mm, depending on the test condition.

The CO_2 mass solubility and the solution mass density were calculated via the PC-SAFT EoS.[25] In this model, the compressibility factor is composed of an ideal gas part (id), a hard-chain part (hc), and a perturbation part (disp) as

$$Z = Z^{\text{id}} + Z^{\text{hc}} + Z^{\text{disp}} \tag{6}$$

where Z^{hc} and Z^{disp} are written in terms of three pure component parameters, that is, the number of segments m_i, the segment diameter σ_i and the segment energy parameter ε_i. In the PC-SAFT EoS employed in this study, only the dispersive attractions were considered.[7] The pure component parameters for CO_2 (m_1, σ_1, and ε_1) used in the present work were those originally determined by Gross and Sadowski[25] via fitting of the vapor pressure and saturated liquid volume data. The pure component parameters for POE ISO 68 oil (m_2, σ_2, and ε_2) were optimized using a simplex Nelder-Mead algorithm via fitting of our own experimental density data at atmospheric pressure (Table 1). The absolute average deviation (to be defined below) associated with the POE ISO 68 density data fit was 0.13%. Associating molecular interactions were not considered in the present analysis.

The van der Waals one-fluid mixing rule was adopted to extend the perturbation theory to the case of mixtures. Conventional Berthelot-Lorentz combining rules were employed to determine the segment diameter, σ_{ij}, and the segment energy parameter, ε_{ij}, for pairs of unlike segments as

$$\sigma_{ij} = \frac{1}{2}(\sigma_i + \sigma_j) \tag{7}$$

$$\varepsilon_{ij} = \sqrt{\varepsilon_i \varepsilon_j}(1 - k_{ij}) \tag{8}$$

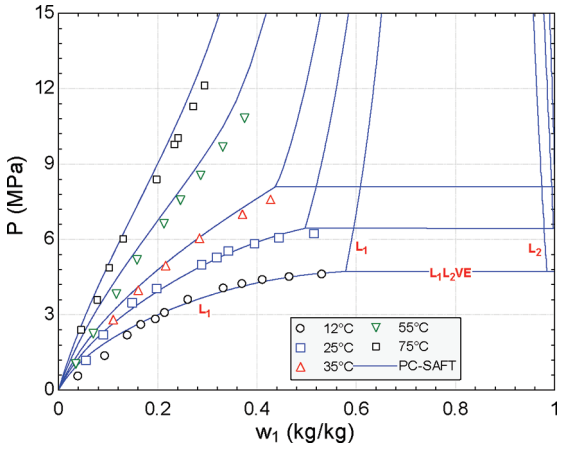

Figure 4. Phase equilibrium diagram of the CO_2−POE ISO 68 system.[7]

where k_{ij} is a binary interaction parameter that accounts for segment−segment interactions of unlike chains. In the present paper, a single temperature dependent interaction parameter was used. This is given by

$$k_{12} = 0.14225 + 0.000158T \tag{9}$$

where T is the absolute temperature (K). The empirical expression in eq 9 was derived from our own experimental phase equilibrium data[7] for the CO_2−POE system.

The bubble point pressure−temperature-solubility diagram for the CO_2−POE system is shown in Figure 4.[7] The solid lines correspond to PC-SAFT EoS predictions with the interaction parameter of eq 9. As can be seen, miscibility gaps are predicted for temperatures below and above the critical temperature of CO_2. Although no experimental data is reported for regions other than that of vapor−liquid equilibrium, the present predictions are in good qualitative agreement with data reported in the literature for similar systems.[1] The root-mean-square (RMS) error and the absolute average deviation (AAD) associated with the prediction of the system pressure by the PC-SAFT EoS are 1.8% and 5.9%, respectively. RMS and AAD are defined as

$$\text{RMS} = \frac{100}{n}\sum_{i=1}^{n}\sqrt{\frac{(\beta_{\text{cal},i} - \beta_{\text{exp},i})^2}{\beta_{\text{exp},i}^2}} \tag{10}$$

$$\text{AAD} = \frac{100}{n}\sum_{i=1}^{n}\left|\frac{\beta_{\text{cal},i} - \beta_{\text{exp},i}}{\beta_{\text{exp},i}}\right| \tag{11}$$

where β is a generic property and n is the total number of data points. The mass diffusivity was calculated considering a thermodynamic factor for nonideal mixtures that takes into account the composition effect.[26] Therefore

$$D_{12} = D_{12}^{\circ}\left(1 + \frac{\partial \ln \varphi_1}{\partial \ln x_1}\right) \tag{12}$$

where φ_1 is the CO_2 fugacity coefficient calculated via the PC-SAFT EoS[25] and x_1 is the CO_2 mole fraction in the liquid. The binary diffusivity at infinite dilution, D_{12}°, was calculated via the Hayduk and Minhas[27] correlation as

$$D_{12}^{\circ} = 1.55 \times 10^{-8}\frac{V_2^{0.27}}{V_1^{0.42}}\frac{T^{1.29}}{\eta_2^{0.92}}\frac{\sigma_2^{0.125}}{\sigma_1^{0.105}} \tag{13}$$

dx.doi.org/10.1021/ie2011752 |Ind. Eng. Chem. Res. 2012, 51, 1027−1035

where T is the absolute temperature (K), V_i is the component molar volume at its normal boiling temperature ($cm^3\ mol^{-1}$), η_i is the component viscosity (cP), and σ_i is the surface tension ($dyn\ cm^{-1}$). The POE viscosity and molar volume were also obtained from our own experimental data,[7] and the normal boiling temperature of the POE ISO 68 oil (751 K) was estimated with the group contribution method of Constantinou and Gani.[28] The surface tension of the oil was calculated with the Brock and Bird corresponding states method.[29] The physical properties of CO_2 were obtained from REFPROP 8.0.[30]

Mass Balance in the Vapor Phase. The instantaneous pressure is determined via a mass balance in the vapor phase. Assuming that the vapor pressure of the oil is negligible and the vapor phase is comprised only of CO_2, a common hypothesis in the analysis of phase equilibrium of refrigerant-oil mixtures[31], one has

$$\frac{1}{A}\frac{dm_G}{dt} = -m''_{I,1} \tag{14}$$

where A is the cross-sectional area of the test cell and $m''_{I,1}$ is the interfacial mass flux of CO_2 with respect to the interface. The mass of CO_2 in the vapor phase is given by

$$\frac{m_G}{A} = \frac{pM_1(L_T - L)}{ZRT} \tag{15}$$

where Z is the compressibility factor of the vapor, R is the universal gas constant, and M_1 is the molecular mass of CO_2. By assuming that the system is isothermal, one has

$$\frac{dp}{dt} = \frac{-RTZm''_{I,1}}{M_1(L_T - L)} + \frac{p}{Z}\frac{dZ}{dt} + \frac{p}{(L_T - L)}\frac{dL}{dt} \tag{16}$$

where the first term on the right corresponds to the pressure decrease because of the interfacial mass flux of CO_2 into the liquid phase. The second term is a gas compressibility correction, with the compressibility factor calculated according to the PC-SAFT EoS.[25] The third term accounts for the variation of pressure because of swelling of the liquid.

Interfacial Mass Balance. The interfacial species balances are given by[32]

$$m''_{I,1} = \rho_{L,1}u_L - \frac{\rho_L D_{12}\partial w_1}{L\ \partial\alpha}\bigg|_{\alpha=0} - \rho_{L,1}\frac{dL}{dt} \tag{17}$$

$$m''_{I,2} = \rho_{L,2}u_L - \frac{\rho_L D_{12}\partial w_2}{L\ \partial\alpha}\bigg|_{\alpha=0} - \rho_{L,2}\frac{dL}{dt} \tag{18}$$

where $\rho_{L,1}$ and $\rho_{L,2}$ are the interfacial mass concentrations of CO_2 and POE, and u_L is the absolute mixture mass velocity. Since the oil does not evaporate, the oil interfacial mass flux is zero. As thermodynamic equilibrium is assumed at the interface

$$w_1^{sat} = 1 - \frac{\rho_{L,2}}{\rho_L} \tag{19}$$

and the mixture mass velocity is given by

$$u_L = \frac{dL}{dt} - \frac{1}{(1 - w_1^{sat})}\frac{D_{12}\partial w_1}{L\ \partial\alpha}\bigg|_{\alpha=0} \tag{20}$$

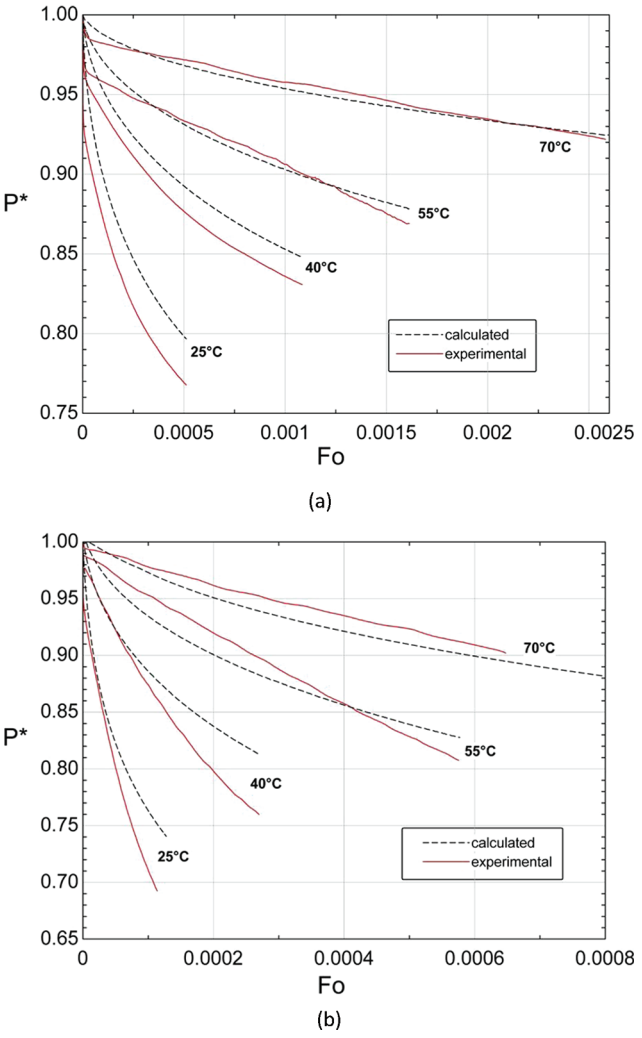

Figure 5. Pressure behavior in the CO2-POE ISO 68 system for an initial liquid height of (a) 37 mm and (b) 74 mm.

substituting eq 20 in eq 17 gives

$$m''_{I,1} = -\frac{\rho_L}{(1 - w_1^{sat})}\frac{D_{12}\partial w_1}{L\ \partial\alpha}\bigg|_{\alpha=0} \tag{21}$$

Height of the Liquid Layer. The instantaneous height of the liquid layer is calculated via the relationship

$$L = \frac{m_2}{\int_0^1 (1 - w_1)\rho_L A\ d\alpha} \tag{22}$$

where m_2 is the mass of oil in the liquid phase, which remains constant during the experiment since the vapor pressure of the oil is assumed negligible.

Numerical Solution Procedure. The numerical solution procedure consists of the following steps:

1. At a given time, t, the system pressure, the height of the liquid layer and the temperature (assumed constant) are known. The initial condition ($t = 0$) for pressure, p_0, is obtained from the experimental data and corresponds to the maximum pressure in the test cell. The initial height of the liquid layer is

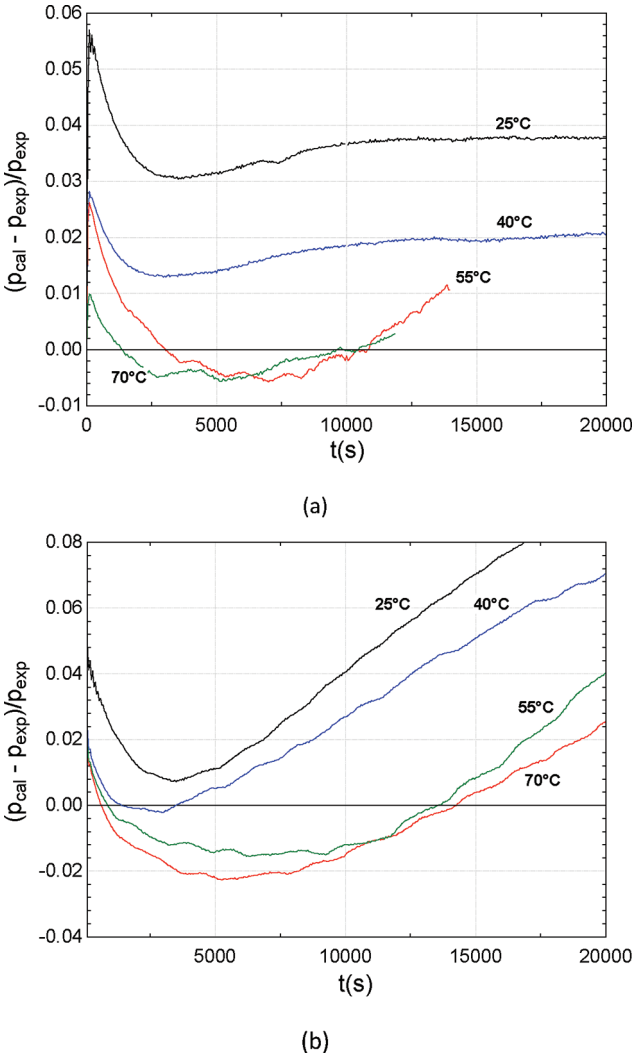

Figure 6. Instantaneous error of the pressure prediction for initial liquid heights of (a) 37 mm and (b) 74 mm.

calculated based on the volume of oil, the cross-section area of the test cell and the oil density. The initial condition for the CO_2 mass fraction in the liquid is given by eq 3.

2. The equilibrium mass fraction (solubility) at the interface, w_1^{sat}, is calculated as a function of the pressure and temperature using the PC-SAFT EoS.[25]
3. The diffusion of CO_2 in the liquid phase is calculated via eqs 1−5, and a new solute mass fraction distribution is obtained for time $t + \Delta t$. The concentration dependence of the liquid density and of the mass diffusivity is taken into account at this stage. The interfacial mass flux is calculated from eq 21, and the updated height of the liquid layer is obtained from eq 22.
4. The system pressure at time $t + \Delta t$ is calculated from eq 16.
5. If t is less than the total integration time, t_f, then return to step 1.

The numerical model was implemented in the Engineering Equation Solver (EES).[33] Equations 1−5 were solved by the finite difference method with a first-order centered difference scheme for the spatial term and a first-order explicit scheme for the temporal term. A constant time step of 50 s was used with a total integration time of 2.0×10^4 s for each run. The height of the liquid layer was divided into 21 equally spaced nodes. Thus, at the beginning of the simulations, the step size was equal to 1.76 mm and 3.52 mm for the 37-mm and 74-mm high oil layers, respectively. Simulations were also carried out with 51 equally spaced nodes,[14] but the smaller mesh was found to be sufficiently accurate, as the average absolute error between model and experiments were marginally affected (less than 0.1%) by the number of grid points. The integral in eq 22 was solved by the trapezoidal rule and the time differentials in eq 16 were calculated via the Euler method.

RESULTS AND DISCUSSION

Figure 5 shows the pressure decay as a function of time for absorption of CO_2 in POE ISO 68 for the two heights of the liquid layer. Pressure was nondimensionalized with respect to the maximum pressure in each test ($P^* = p/p_0$) and time was nondimensionalized as a mass transfer Fourier number ($Fo = tD_{12}^0/L^2$)). As the solubility is the driving force for mass transfer, the rate of pressure decrease was inversely proportional to the system temperature. An abrupt decay in pressure was observed for the experimental data at the very initial instants of mass absorption. Although the data trend was well picked up by the model, the sharp decay, which was more apparent for the 37 mm case, was not accurately predicted by the model. Although no visual observation of the gas injection in the test section was possible, it was hypothesized that the sharp pressure decay was related to a disruption of the gas−liquid interface as the gas entered the test section and filled up the vapor space. Since the reservoir pressure was many times greater than the initial pressure in the vapor space, the vapor expanded and entered the test section with a high velocity through the 3.8-mm ID inlet port. Thus, the mass transfer rate at the beginning of the absorption process became more pronounced possibly due to turbulence in the vapor and in the liquid and to an increase of the interfacial area due to interface roughening associated with the gas flow.

At the four temperatures evaluated, thermodynamic equilibrium was not reached before the end of the test (about 2×10^4s). Figure 6 shows the error associated with the instantaneous pressure predicted by the mathematical model. As can be seen, the errors tend to be larger for the initial instants of absorption before reaching a minimum at intermediate times and increasing again. Larger instantaneous errors are seen at the lower temperatures. The average absolute error associated with the pressure prediction over the whole interval was less than 4% for all cases (see Table 2). Table 2 also presents the mass of CO_2 that entered the test cell in each run and the maximum (initial) pressure for each run. The mass of carbon dioxide entering the cell is inversely proportional to the system temperature (due to expansion of the gas) and to the height of the liquid layer (due to the smaller space available for the gas).

Figure 7 shows the temperature profiles during the initial stages of each test for the 37 mm case. The temperature behavior for the 74 mm case was similar. Initially, due to the latent heat of absorption and the high rates of mass transfer, there was a significant temperature increase in the vapor and at the interface. The temperature of the liquid did not undergo a major change due to the large specific heat of the oil.

An explanation is in order for the observed differences between the temperatures in the liquid and vapor phases and the

dx.doi.org/10.1021/ie2011752 |Ind. Eng. Chem. Res. 2012, 51, 1027–1035

Table 2. Experimental Conditions and Model Predictions

height of the liquid layer (mm)	T (°C)	p_0 (kPa)	$m_{1,T}$ (g)	average absolute deviation (complete model) (%)	average absolute deviation (ideal model) (%)
37	25	5214	183.94	3.6	29.8
37	40	5170	167.51	1.8	21.3
37	55	5079	146.09	0.5	10.1
37	70	5016	135.49	0.3	6.7
74	25	5565	150.41	3.9	21.4
74	40	5540	137.30	3.0	19.3
74	55	5502	119.95	1.4	14.0
74	70	5465	109.76	1.3	5.8

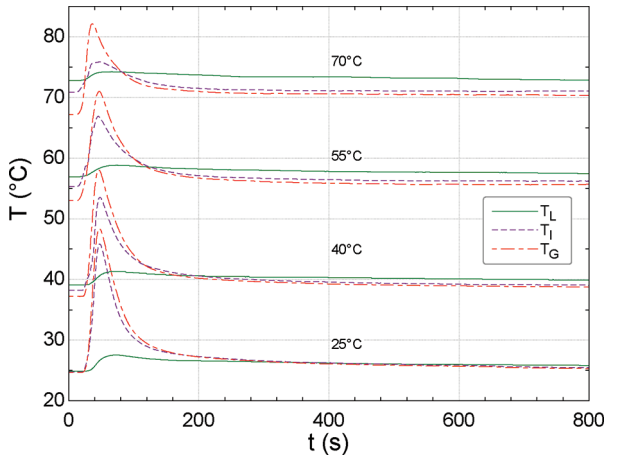

Figure 7. Temperature behavior in the CO2-POE ISO 68 system for an initial liquid height of 37 mm.

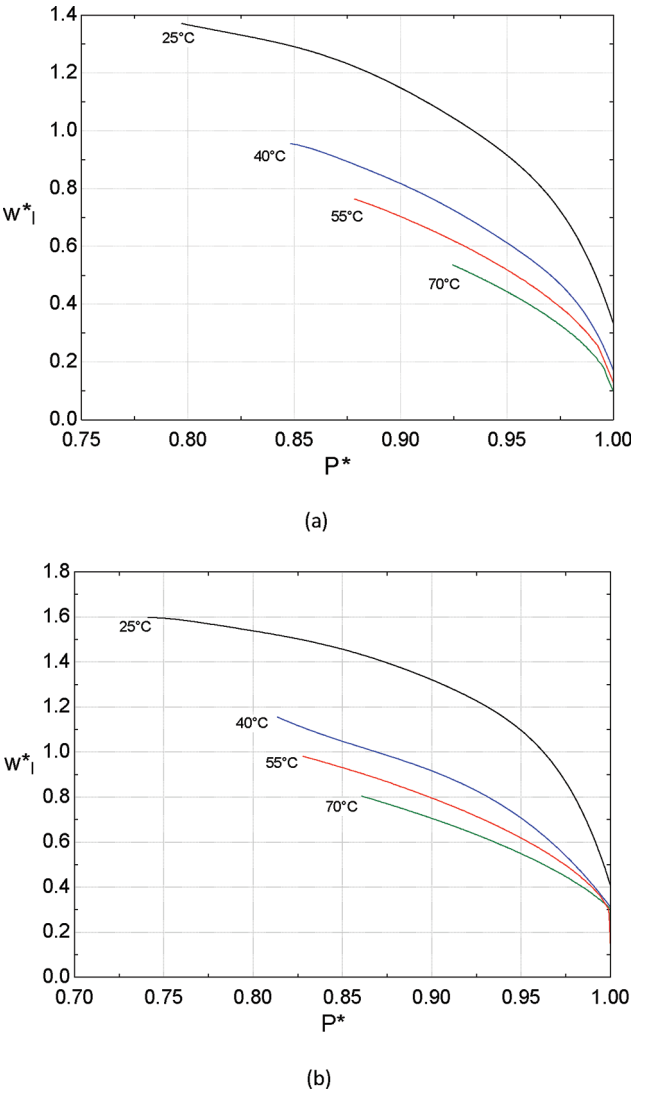

Figure 8. Behavior of the normalized CO_2 interfacial mass fraction as a function of pressure (dimensionless) and temperature. Initial liquid height of (a) 37 mm and (b) 74 mm.

temperature near the interface before starting the experiment. As can be seen, the differences are quite small for the 25 °C case, but tend to increase with increasing temperature. In the experiments, the test section lid (that is bolted via a flat face flange to the main body of the test section) was located right at the water line (see schematic diagram in Figure 1) and, because of that, it was at a temperature closer to that of the ambient air. In tests where the water temperature in the tank was significantly higher than the ambient temperature, a temperature gradient was generated inside the test section, which may have resulted in a significant heat exchange between the oil−vapor interface, the inner surface of the lid and the temperature sensors (mainly by radiation). It is believed, however, that the existence of this temperature gradient does not alter the main conclusions of the model (that relies on the assumption of a constant temperature in the system). In fact, the temperature signals shown in Figure 7 serve to illustrate that after the initial temperature excursion due to the intense latent heat release at the interface, the temperatures return to the baseline values for each test, justifying the assumption of constant temperature in the diffusion model.

Another point worthy of note in Figure 7 is related to the fact that the gas temperature was consistently higher than the interface temperature. In this respect, it should be mentioned that it was not possible to guarantee that the tip of the RTD measured the temperature *exactly* at the interface. Even if the tip of the sensor were just a couple of millimeters below the interface (which rises continuously as a result of swelling), the local temperature reading would already be influenced by the liquid thermal diffusivity. Moreover, for the higher temperatures, there might also have been an effect due to thermal radiation exchange between the walls of the test section and the temperature sensor in the vapor space. The characteristics of this radiative transfer are certainly different from that between the walls and the "interface"

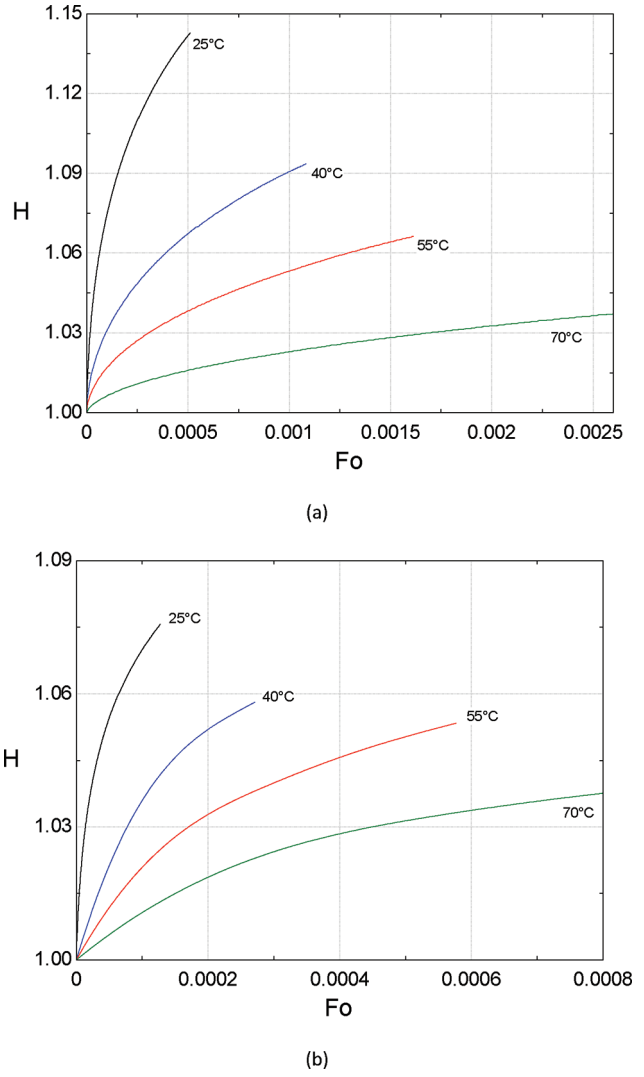

Figure 9. Increase of the height of the liquid layer as a result of liquid swelling. Initial height of the liquid layer: (a) 37 and (b) 74 mm.

RTD due to the different thermal properties of the two media.

Figure 8 shows the interfacial mass concentration as a function of the normalized pressure. The interfacial mass concentration was nondimensionalized as

$$w_1^* = \frac{w_1^{\text{sat}}(p,T)}{w_1^{\text{id}}(p,T)} \tag{23}$$

where $w_1^{\text{sat}}(p,T)$ is the interfacial mass fraction calculated with the PC-SAFT EoS and $w_1{}^{\text{id}}(p,T)$ was calculated with Raoult's Law (ideal solution hypothesis). As can be seen, considerable deviations with respect to the ideal solution behavior for the interfacial concentration occur at all temperatures. At the beginning of the absorption process (high dimensionless pressures), the ideal solution model grossly underestimates the interfacial mass fraction, and the negative deviation with respect to Raoult's law becomes more pronounced as the temperature increases. For a given temperature, as the pressure decreases due to CO_2 absorption in the liquid, the magnitude of the deviation decreases. For the lowest temperatures, a mixed deviation is observed as the interfacial mass fraction becomes larger than that calculated via Raoult's law. This complex behavior was somewhat expected due to the nature of the CO_2−POE ISO 68 system. An in-depth study of the phase equilibrium of mixtures involving CO_2 and synthetic oils[7] has predicted the occurrence of miscibility gaps, i.e, regions of VLLE (vapor−liquid−liquid equilibrium), at temperatures below and above the critical temperature of CO_2, as shown in Figure 4. However, it should be noted that all conditions evaluated in the present study correspond to situations of vapor−liquid equilibrium, that is, on the lines labeled as L_1 in Figure 4.

Figure 9 presents the increase in the liquid height as a function of time resulting from liquid swelling. Time was nondimensionalized in terms of the mass transfer Fourier number. The nondimensionalized height is defined as

$$H = \frac{L}{L_0} \tag{24}$$

where L is the instantaneous height of the liquid layer and L_0 is the initial height of pure oil layer. It can be observed that the swelling of the liquid was more pronounced at lower temperatures, since more CO_2 dissolved into the oil at these conditions. For the 37 mm case, the liquid swelling was more pronounced, and the height of the liquid phase increased almost 15% at 25 °C and 3% at 70 °C at the end of the experiment.

Two effects are accounted for in the swelling of the liquid layer, that is, the volume of carbon dioxide that dissolves in the oil and the volume change due to mixing of the two components. If, at thermodynamic equilibrium, the difference between the two volumes is zero, then the excess volume is also zero and the liquid mixture behaves as an ideal solution. At the end on an experimental run, the fraction of the nondimensionalized height of the liquid layer associated with the mixing of the components is given by

$$H^{\text{mix}} = H - H^{\text{id}} \tag{25}$$

where, for temperatures below the critical temperature of carbon dioxide, the ideal part of the nondimensionalized height is given by

$$H^{\text{id}} = \frac{1}{AL_0}[v_{1,\text{L}}(m_{1,\text{T}} - m_{\text{G},f}) + v_2 m_2] \tag{26}$$

The mass of the vapor region (assumed to be pure carbon dioxide) at the end of an experimental run is given by

$$m_{\text{G},f} = \frac{A}{v_{\text{G}}}(L_{\text{T}} - L_f) \tag{27}$$

In the above equations, v_2 is the specific volume of POE ISO 68, $v_{1,\text{L}}$ is the specific volume of CO_2 as saturated liquid at the system temperature,[30] $m_{1,\text{T}}$ is the mass of CO_2 that entered the test section (determined experimentally), and v_{G} is the specific volume of the vapor evaluated at p_f and T,[30] where p_f is the system pressure at the end of the experiment. For the 25 °C experimental runs (37 and 74 mm), the values of H, H^{id}, and H^{mix} are 1.143, 1.127, and 0.016 (37 mm) and 1.076, 1.084, and −0.008 (74 mm), respectively. As can be seen, the volume change due to mixing is much smaller than the volume of liquid carbon dioxide that dissolves in the POE ISO to the oil. This effect is related to the differences in molecular size between the components and is quantified via the intermolecular (dispersion) forces calculated by the PC-SAFT EoS.[25] However, the figures associated with the ideal and mixing part contributions to

swelling should be viewed with a certain caution, since the system had not reached thermodynamic equilibrium at the end of the experimental runs.

As a whole, the consideration of "non-ideal" effects contributes significantly to improving the prediction ability of the diffusion model. Here, the term "ideal" has been used to symbolize, in the context of the mass diffusion model, the adoption of the following assumptions: (i) the interfacial equilibrium mass fraction (solubility) was calculated using Raoult's law; (ii) the liquid mass density is calculated using the ideal solution (additive volumes) hypothesis; (iii) the mass diffusivity is assumed constant and equal to the infinite dilution mass diffusivity, D_{12}^{0}, calculated via the Hayduk and Minhas (1982) correlation; (iv) the liquid height is held constant (no liquid swelling). The sixth column of Table 2 presents the average absolute deviations associated with the pressure prediction assuming ideal behavior. The ideal model severely under-predicts the instantaneous pressure because of the ideal interfacial mass fractions are higher than those obtained via the PC-SAFT EoS,[25] which give rise to higher interfacial mass fluxes.

CONCLUSIONS

Absorption of CO_2 through the free surface of a stagnant layer of POE ISO 68 lubricant oil was investigated in this paper via the pressure decay method. An experimental facility was constructed to measure the system pressure, the mass of CO_2 that enters the PVT cell at each test and the temperatures of the liquid, vapor and interface regions. Experiments were carried out for two distinct initial heights of the liquid layer (37 and 74 mm). A transient mass diffusion model which took into account nonideal effects via the PC-SAFT EoS,[25] namely, (i) gas compressibility in the vapor phase, (ii) liquid phase swelling and nonideal concentration-dependent density behavior, (iii) nonideal ELV equilibrium at interface, and (iv) concentration-dependent mass diffusivity, was implemented. The main findings of the study are as follows:

1. The mathematical model produced results that are in good agreement with the experimental data for the pressure decay. The minimum and maximum average absolute deviations were 0.3% and 3.9%, respectively. The agreement between the model and the data improves as the system temperature increases.
2. Swelling of the liquid layer was significant, and increased with decreasing temperatures due to the fact that the mass transfer potential is inversely proportional to temperature. At 25 °C, for the 37 mm case, the height of the liquid layer increases almost by 15% after 2×10^4 s. The volume change due to mixing of carbon dioxide and POE ISO 68 was found to be much smaller that the volume of liquid carbon dioxide that dissolves in the oil.
3. "Non-ideal" effects have proven to be crucial for an accurate determination of the pressure decay by CO_2 diffusion in the liquid. If liquid swelling is neglected, a constant liquid phase mass density and a constant mass diffusivity are assumed and Raoult's law is used to calculate the interfacial mass fraction (solubility), the average absolute deviations of the instantaneous system pressure during absorption can be as large as 30%.

AUTHOR INFORMATION

Corresponding Author

*Phone/Fax: + 55 48 3234 5166. E-mail: jrb@polo.ufsc.br.

ACKNOWLEDGMENT

The material presented in this paper is a result of a long-standing technical-scientific partnership between UFSC and Embraco. Financial support from FINEP and CNPq through grant No. 573581/2008-8 (National Institute of Science and Technology in Cooling and Thermophysics) is duly acknowledged.

NOTATION

A = area (m^2)
D_{12} = diffusion coefficient ($m^2\ s^{-1}$)
Fo = mass transfer Fourier number
H = normalized height of the liquid layer
L = height of liquid layer (m)
L_T = height of test cell (m)
k_{ij} = interaction parameter
m = mass (kg)
m_i = number of segments
m_2 = mass of oil in the liquid (kg)
M_i = molecular mass of component i ($kg\ kmol^{-1}$)
$m''_{l,1}$ = mass flux of CO_2 with respect to the interface ($kg\ m^{-2}\ s^{-1}$)
p = pressure (Pa)
t = time (s)
T = temperature (K)
R = Universal gas constant ($J\ kmol^{-1}.K^{-1}$)
v = specific volume ($m^3\ kg^{-1}$)
V_i = molar volume of component i ($m^3\ kmol^{-1}$)
w_i = mass fraction of component i ($kg\ kg^{-1}$)
x_i = mole fraction of component i ($kmol\ kmol^{-1}$)
z = distance (m)
Z = compressibility factor

Greek Letters

α = normalized distance
ε_i = segment energy parameter (J)
φ_i = fugacity coefficient of component i
η = viscosity (Pa s)
ρ = mass density ($kg\ m^{-3}$)
$\rho_{L,i}$ = mass concentration of component i in the liquid ($kg\ m^{-3}$)
σ = surface tension ($N\ m^{-1}$)
σ_i = segment diameter (Å)

Subscripts

0 = initial value
1 = carbon dioxide
2 = POE ISO 68
f = final value
G = vapor
I = interface
i = component i
j = component j
L = liquid
T = total

Superscripts

° = infinite dilution
id = ideal
mix = mixture

sat = saturation (equilibrium)
* = normalized variable

REFERENCES

(1) Hauk, A.; Weidner, E. Thermodynamic and Fluid-Dynamic Properties of Carbon Dioxide with Different Lubricants in Cooling Circuits for Automobile Application. *Ind. Eng. Chem. Res.* **2000**, *39*, 4646.

(2) Tsuji, T.; Tanaka, S.; Hiaki, T.; Saito, R. Measurements of Bubble Point Pressure for CO_2 + Decane and CO_2 + Lubricating Oil. *Fluid Phase Equilib.* **2004**, *219*, 87.

(3) Yokozeki, A. Solubility Correlation and Phase Behaviour of Carbon Dioxide and Lubricant Oil Mixtures. *Applied Energy* **2007**, *84*, 159.

(4) Fedele, L.; Bobbo, S.; Pernechele, F.; Stryjek, R. Solubility Temperature Dependence and Data Correlation of Carbon Dioxide in Pentaerythritol Tetra-2-Methylbutyrate. *J. Chem. Eng. Data* **2009**, *54*, 3104.

(5) García, J.; Paredes, X.; Fernández, J. Phase and Volumetric Behaviour of Binary Systems Containing Carbon Dioxide and Lubricants for Transcritical Refrigeration Cycles. *J. Supercrit. Fluids* **2008**, *45*, 261.

(6) García, J.; Youbi-Idrissi, M.; Bonjour, J.; Fernández, J. Experimental and PC-SAFT Volumetric and Phase Behaviour of Carbon Dioxide + PAG or POE Lubricant Systems. *J. Supercrit. Fluids* **2008**, *47*, 8.

(7) Marcelino Neto, M. A.; Barbosa, J. R., Jr. Phase and Volumetric Behaviour of Mixtures of Carbon Dioxide (R-744) and Synthetic Oils. *J. Supercrit. Fluids* **2009**, *50*, 6.

(8) Fukuta, M.; Yanagisawa, T.; Shimizu, T.; Nishijima, H. Transient Mixing Characteristics of Refrigerant with Refrigerant Oil. *Proc. 19th. Int. Congress Refrig., IVa* **1995**, 215–222.

(9) Goswami, D. Y.; Shah, D. O.; Jotshi, C. K.; Bhagwat, S. S.; Leung, M.; Gregory, A. S.; Lu, S. *Foaming Characteristics of Refrigerant/Lubricant Mixtures*; ARTI-MCLR Report 665-53200; US DOE: Washington, DC, 1998.

(10) Leung, M.; Jotshi, C. K.; Goswami, D. Y.; Shah, D. O.; Gregory, A. Measurements of Absorption Rates of HFC Single and Blended Refrigerants in POE Oils. *HVAC&R Res.* **1998**, *26*, 141.

(11) Yokozeki, A. Time-Dependent Behavior of Gas Absorption in Lubricant Oil. *Int. J. Refrig.* **2002**, *25*, 695.

(12) Gessner, T. R.; Barbosa, J. R., Jr. Modeling Absorption of Pure Refrigerants and Refrigerant Mixtures in Lubricant Oil. *Int. J. Refrig.* **2006**, *29*, 773.

(13) Barbosa, J. R., Jr.; Thoma, S. M.; Marcelino Neto, M. A. Prediction of Refrigerant Absorption and Onset of Natural Convection in Lubricant Oil. *Int. J. Refrig.* **2008**, *31*, 1231.

(14) Marcelino Neto, M. A.; Barbosa, J. R., Jr. Absorption of Isobutane (R-600a) in Lubricant Oil. *Chem. Eng. Sci.* **2011**, *66*, 1906.

(15) Fukuta, M.; Yanagisawa, T.; Omura, M.; Ogi, Y Mixing and Separation Characteristics Of Isobutane With Refrigerant Oil. *Int. J. Refrig.* **2005**, *28*, 997.

(16) Barbosa, J. R., Jr.; Ortolan, M. A. Experimental and Theoretical Analysis Of Refrigerant Absorption In Lubricant Oil. *HVAC&R Res.* **2008**, *14*, 141.

(17) Peng, D. Y.; Robinson, D. B. A New Two-Constant Equation of State. *Ind. Eng. Chem.* **1976**, *15*, 59.

(18) Tharanivasan, A. K.; Yang, C.; Gu, Y. Comparison of Three Different Interface Mass Transfer Models Used in the Experimental Measurement of Solvent Diffusivity in Heavy Oil. *J. Pet. Sci. Eng.* **2004**, *44*, 269.

(19) Sheikha, H.; Mehrotra, A. K.; Pooladi-Darvish, M. An Inverse Solution Methodology for Estimating the Diffusion Coefficients of Gases in Athabasca Bitumen from Pressure-Decay Data. *J. Pet. Sci. Eng.* **2006**, *53*, 189.

(20) Rasmussen, M. L.; Civan, F. Parameters of Gas Dissolution in Liquids Obtained by Isothermal Pressure Decay. *AIChE J.* **2009**, *55*, 9.

(21) Okhotsimskii, A.; Hozawa, M. Schlieren Visualization of Natural Convection in Binary Gas-Liquid Systems. *Chem. Eng. Sci.* **1998**, *53*, 2547.

(22) Shiflett, M. B.; Yokozeki, A. Solubilities and Diffusivities of Carbon Dioxide in Ionic Liquids: [bmim][PF6] and [bmim][BF4]. *Ind. Eng. Chem. Res.* **2005**, *44*, 4453.

(23) Huang, J.; Rüther, T. Why Are Ionic Liquids Attractive for CO_2 Absorption? An Overview. *Aust. J. Chem.* **2009**, *62*, 298.

(24) Liu, H.; Huang, J.; Pendleton, P. Experimental and Modelling Study of CO_2 Absorption in Ionic Liquids Containing Zn (II) Ions. *Energy Proced.* **2011**, *4*, 59.

(25) Gross, J.; Sadowski, G. Perturbed-Chain SAFT: An Equation of State Based on a Perturbation Theory for Chain Molecules. *Ind. Eng. Chem. Res.* **2001**, *40*, 1244.

(26) Riazi, M. R. A New Method for Experimental Measurement of Diffusion Coefficients in Reservoir Fuids. *J. Pet. Sci. Eng.* **1996**, *14*, 235.

(27) Hayduk, W.; Minhas, B. S. Correlations for Prediction of Molecular Diffusivities in Liquids. *Can. J. Chem. Eng.* **1982**, *60*, 295.

(28) Constantinou, L.; Gani, R. New Group Contribution Method for Estimating Properties of Pure Compounds. *AIChE J.* **1994**, *40*, 1697.

(29) Poling, B. E.; Prausnitz, J. M.; O'Connell, J. P. *The Properties of Gases and Liquids*; McGraw-Hill: New York, 2000.

(30) Lemmon, E. W.; Huber, M. L.; McLinden, M. O. *REFPROP 8.0*, NIST Standard Reference Database 23; NIST: CO, 2007.

(31) Lubricants in Refrigerant Systems. *ASHRAE Handbook—Refrigeration*; ASHRAE: Atlanta, GA, 2010; Chapter 12.

(32) Deen, W. M. *Analysis of Transport Phenomena*; Oxford University Press: Oxford, U.K., 1998.

(33) Klein, S. A. *Engineering Equation Solver*, professional version V8.775; F-Chart Software: Madison, WI, 2011.